JOURNAL OF MATERIALS SCIENCE 28 (1993) 2943–2949

Creep fracture in Al–SiC metal-matrix composites

A. B. PANDEY, R. S. MISHRA, Y. R. MAHAJAN
Defence Metallurgical Research Laboratory, Kanchanbagh, Hyderabad 500 258, India

Creep fracture behaviour of pure aluminium-matrix composites with 10–30 vol % SiC particulates at 623 K is reported. A comparison of tensile and compression creep data shows the existence of a "transition stress". Above this transition stress no steady state creep is observed in tension. This transition stress is related to a transition from intergranular to transgranular fracture. The origin of transition stress is perhaps associated with the diffusional relaxation of stress concentration at the matrix/particle interface by lattice diffusion. The intergranular creep fracture of composites appears to be similar to that of unreinforced aluminium and it is power-law creep controlled. The transgranular creep fracture occurs by void nucleation and growth. The nucleation strain for voids is quite small and hence the tertiary stage starts before the end of the primary stage. The ductile fracture models overestimate the strain to fracture and do not predict the observed stress dependence of strain to fracture.

1. Introduction

During the last decade, research on metal-matrix composites (MMCs) has received considerable attention because they constitute a new class of materials with a unique combination of higher specific modulus and higher specific strength as compared to the base metals/alloys [1–4]. At present MMCs based on the Al–SiC system are considered as candidates for high-temperature applications, where creep behaviour of the material plays an important role. Although a number of studies are available on the creep deformation of composites [5–15], the overall understanding is poor, and several anomalies exist in the literature. One of the most important anomalies is related to the existence of a proper steady state in the composite. Nieh *et al.* [8] have pointed out that a proper steady-state region exists only for 6061-Al alloy-based composite but not for the 2124-Al-based composites. In a tensile creep study of 2124 Al–20 vol % SiC_w (whisker) composite, Barth *et al.* [12] have reported that a well-defined steady-state creep exists only below a certain stress, referred to by them as the threshold stress (this threshold stress is different from that which is usually used in creep terminology to represent a minimum stress required to produce appreciable deformation). Under such circumstances, it is very difficult to identify the operative steady-state creep mechanisms in composites.

Recently, we have made attempts to resolve some of these problems by comparing tensile and compressive creep behaviour of Al–10 vol % SiC_p (particulate) composite [16], which suggests that in tension a true steady-state regime exists only below the "transition stress" (similar to the threshold stress of Barth *et al.* [12]), whereas in compression it exists at all the stresses. As a result, the minimum creep rate data obtained in tension do not always correspond to the steady-state creep rate. Therefore, if a proper steady state does not exist, only the compression creep data can be analysed for a meaningful evaluation of steady-state creep mechanisms [17]. In addition, we have re-analysed the tensile creep data on 6061/20 vol % SiC_w composites [6, 9] to understand the steady-state creep mechanism [18].

The transition stress is expected to be related to the premature onset of fracture mechanisms during tensile creep testing of composites [16]. Although the fracture of composites at room temperature has attracted considerable attention in the recent past, no significant study has been reported on the creep fracture. In this paper, we report the influence of volume fraction of reinforcement on the creep fracture of Al–SiC composites. A comparison with our previously reported compression-creep data [17] gives the values of the transition stress. The origin of this transition stress is discussed here in terms of operative fracture mechanisms.

2. Experimental procedure

In the present study, three aluminium-matrix composites with 10, 20 and 30 vol % 1.7 μm SiC particulates were used. These composites were made by the powder metallurgy (P/M) route using atomized aluminium (99.6% purity) powder of 45 μm average size and silicon carbide particulates. Silicon carbide particulates of 1.7 μm size were received from Superior Graphite Co., USA. The P/M route involved blending of aluminium and SiC powders followed by cold isostatic pressing at 200 MPa. These compacts were

0022–2461

then sealed in aluminium cans and section rolled at 873 K to produce fully dense composite rods of 12 mm diameter. The rolled rods were annealed at 873 K for 20 h before creep testing.

Samples with 25 mm gauge length and 5 mm diameter were tested in tension using constant-load creep machines. The elongation of the sample was measured using two parallel linear variable displacement transducers (LVDTs), which were mounted on the ridges provided on the sample. The temperature of the sample was monitored using three separate thermocouples tied, one at the sample and the other two at the grips. The specimen temperature was controlled to within $\pm$ 1 K. Scanning electron microscopy (SEM) was used for microscopy and fractography.

3. Results

Fig. 1 shows a fairly uniform distribution of silicon carbide particulates in the Al–20 vol % SiC_p composite. Details of the test conditions and summary of creep results are given in Table I. The creep curves of Al–10 vol % SiC_p composite tested in tension at 623 K

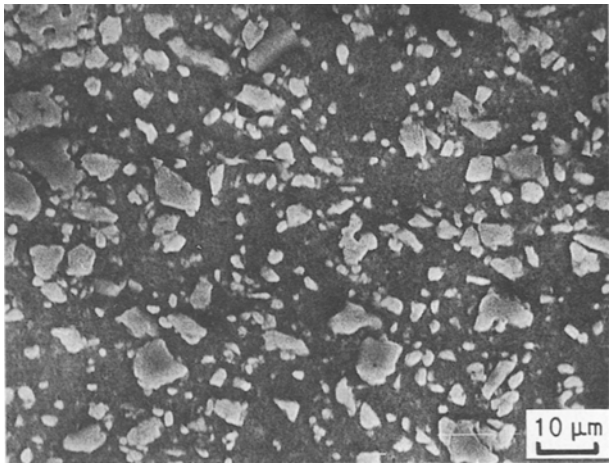

Figure 1 Scanning electron micrograph of Al–20 vol % SiC_p showing uniform distribution of SiC particulates.

are shown in Fig. 2a and b. The creep curve at 24.5 MPa exhibits all three stages (a primary stage where the creep rate decreases with time, a well-defined steady-state stage where the creep rate is essentially constant, and a tertiary stage where the creep rate continuously increases up to fracture) as expected for any material (Fig. 2a). Further, the creep curves at lower stresses consist of a proper steady-state region followed by a very small tertiary stage. However, at higher stresses, a well-defined steady-state region does not exist for any of these composites, as the tertiary stage starts much before the end of the primary stage. As a result, the creep curves at higher stresses are essentially dominated by the tertiary stage (Fig. 2b). The shape of the tertiary part of the creep curve varies significantly with the volume fraction of silicon carbide particulates. As shown in Fig. 2c, the creep curves of 20 and 30 vol % SiC_p have a very small tertiary stage even at higher stresses. From Fig. 3, which plots instantaneous creep rate, $\dot{\varepsilon}_i$, versus normalized time, t/t_f, the early onset of the tertiary stage, starting much before the end of the primary stage can be noted. This completely masks the steady-state region.

Fig. 4 shows a comparison between tension and compression creep for Al–SiC_p composites at 623 K on $\dot{\varepsilon}^{1/8}$ versus σ plots. As is evident from this figure, the minimum creep-rate data of tension deviate significantly from the linearity of the steady-state creep-rate data of compression above a particular stress, referred to as the "transition stress" (it should be noted that the true stress exponent observed for the steady-state creep was 8 [17] and therefore a linear relation is expected between $\dot{\varepsilon}^{1/8}$ and σ). Below this stress, however, there is no difference between the two. The transition stress observed in the present study is summarized in Table II. The transition stress is found to increase with increasing volume fraction.

The fractographs of the Al–10 vol % SiC_p composite tested at 623 K under two stress conditions, one below the transition stress (26 MPa; Fig. 5a) and the other above the transition stress (29 MPa; Fig. 5b) are shown, respectively. The fractograph of the specimen

TABLE I Summary of the creep results of Al–SiC_p composites at 623 K

	Applied stress, σ (MPa)	Minimum creep rate, $\dot{\varepsilon}_m$ (s^{-1})	Time to fracture, t_f (h)	Strain to fracture, ε_f (%)
Al–10 vol % SiC_p	24.5	3.0×10^{-9}	450.0	1.8
	26.4	2.3×10^{-8}	92.0	2.1
	28.5	1.1×10^{-7}	39.8	5.1
	29.0	1.8×10^{-7}	21.5	6.7
	30.5	1.3×10^{-6}	4.8	15.3
Al–20 vol % SiC_p	36.0	7.5×10^{-10}	366.8	0.37
	38.0	4.3×10^{-9}	181.1	0.61
	40.0	2.1×10^{-8}	31.8	0.50
	42.0	4.9×10^{-8}	11.25	0.48
	44.0	8.5×10^{-7}	2.3	1.16
Al–30 vol % SiC_p	48.5	5.0×10^{-10}	Terminated after 914 h	
	50.0	2.2×10^{-8}	40.3	0.58
	52.0	1.9×10^{-8}	34.5	0.47
	54.0	1.7×10^{-6}	0.87	0.84

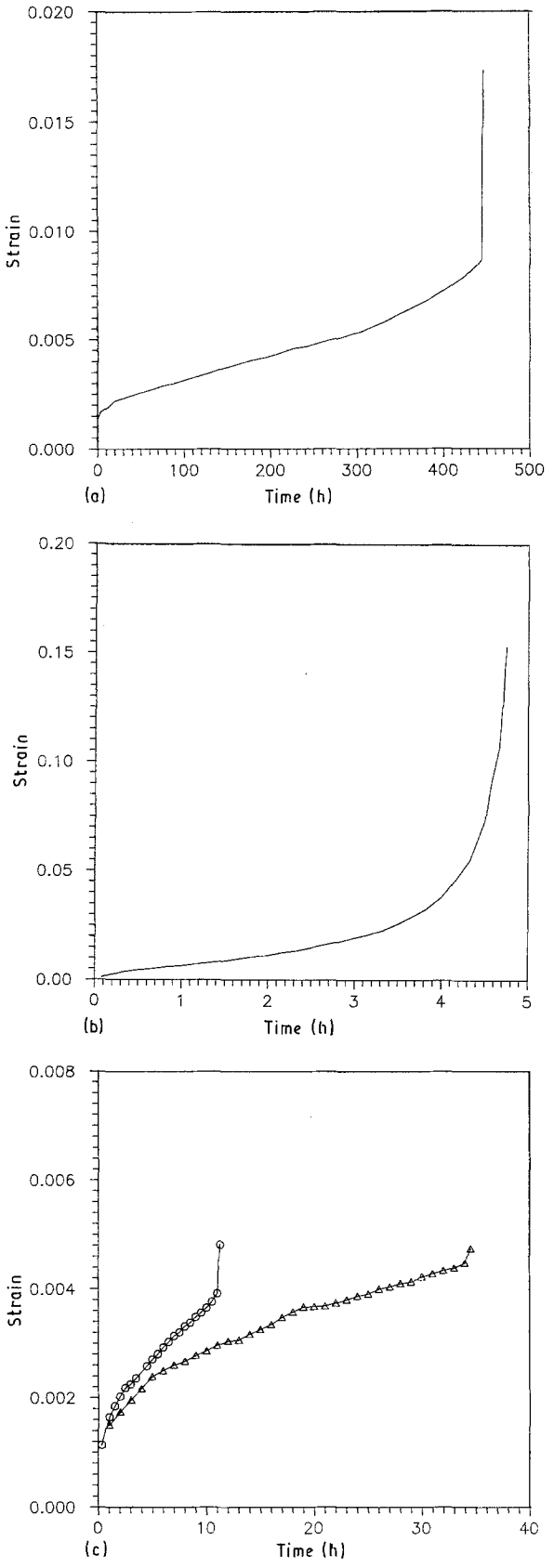

Figure 2 Creep curves at 623 K of (a) Al–10 vol % SiC_p at 24.5 MPa, (b) Al–10 vol % SiC_p at 30.5 MPa, and (c) (○) Al–20 vol % SiC_p at 42 MPa and (△) Al–30 vol % SiC_p at 52 MPa.

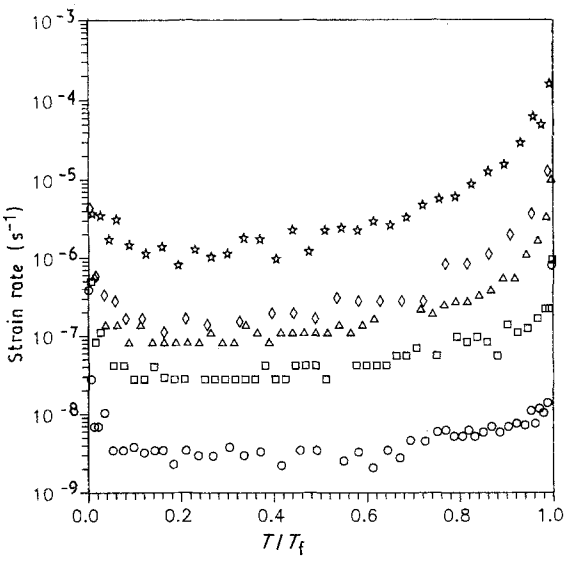

Figure 3 Variation of instantaneous strain rate with normalized time for Al–10 vol % SiC_p composite at 623 K and at various stresses: (○) 24.5 MPa, (□) 26.4 MPa, (△) 28.5 MPa, (◇) 29.0 MPa (☆) 30.5 MPa.

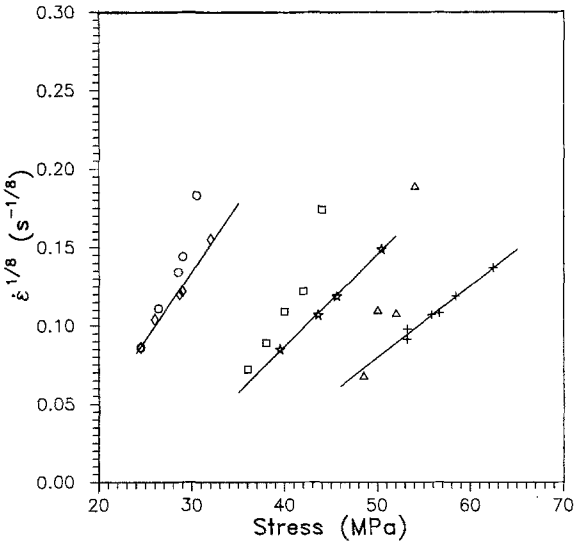

Figure 4 A plot of $\dot{\varepsilon}^{1/8}$ versus σ comparing tension and compression data at 623 K. The stress level at which the tensile data begin to deviate from the compression data is taken as the transition stress. Al–10 vol % SiC, (○) tension, (◇) compression [17]; Al–20 vol % SiC, (□) tension, (☆) compression [17]; Al–30 vol % SiC, (△) tension, (+) compression [17].

TABLE II Transition stress, σ_{tr}, values for Al–SiC_p composites obtained by comparison of tensile and compression creep data

SiC_p (vol %)	Transition stress (MPa)	$(\sigma_{tr} - \sigma_o)/G$[a]
0[b]	12.0	5.7×10^{-4}
10	26.0	4.9×10^{-4}
20	34.8	3.5×10^{-4}
30	48.6	4.7×10^{-4}

[a] Values for σ_o have been taken from [17].
[b] The value for commercial purity aluminium has been taken from Ashby *et al.* [27].

tested at 26 MPa shows a predominantly intergranular failure. On the other hand, at higher stress, the fractograph shows numerous dimples with extensive plastic deformation of the aluminium matrix before fracture, as expected for the transgranular fracture. Further, most of these dimples are associated with SiC particulates suggesting that the Al/SiC_p interface could be a preferential site for cavity nucleation. This

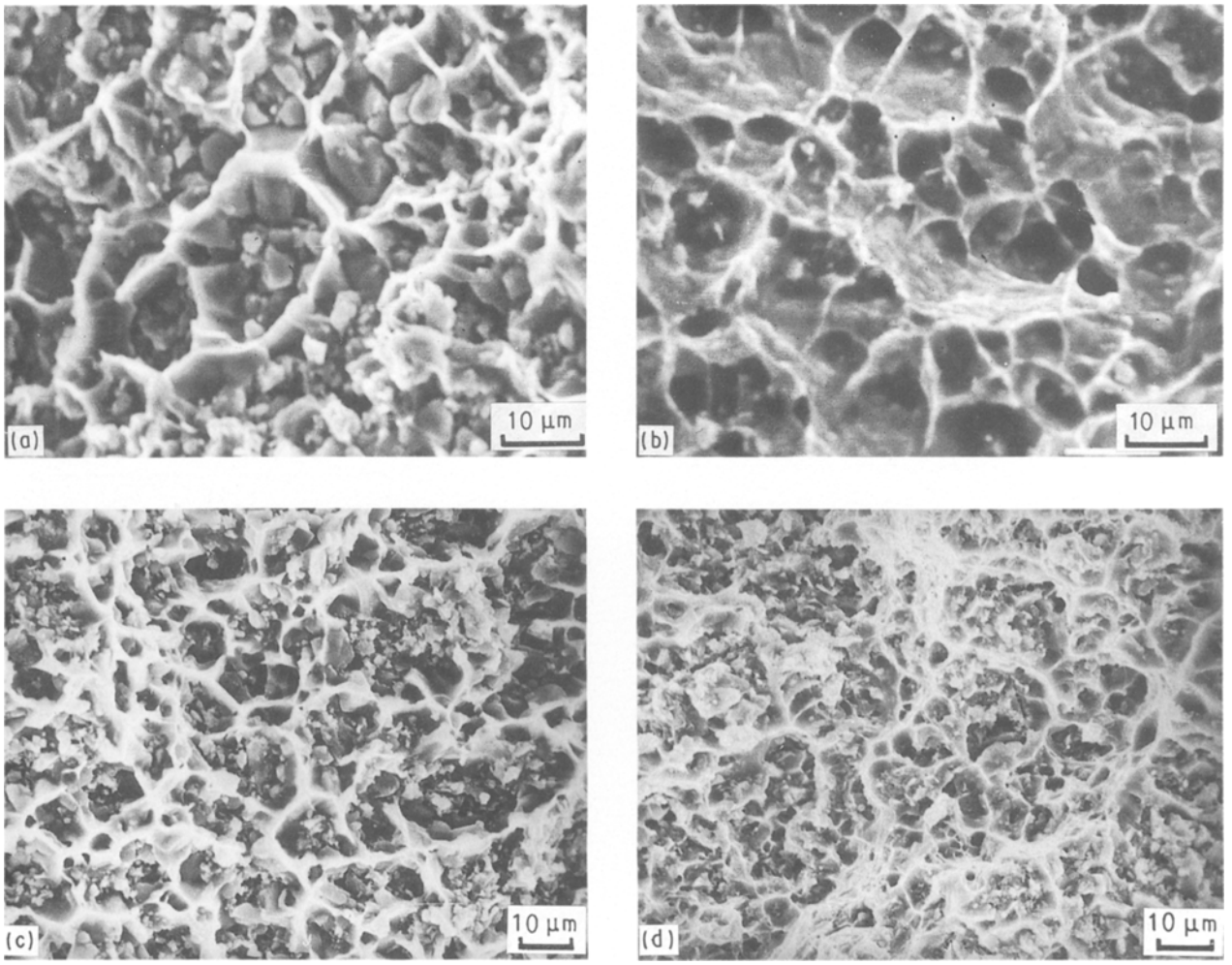

Figure 5 Fractographs of Al–SiC_p composites tested at 623 K: (a) Al–10 vol % SiC_p tested at 26.4 MPa showing predominantly intergranular fracture (below the transition stress), (b) Al–10 vol % SiC_p tested at 29.0 MPa showing transgranular fracture (above the transition stress), (c) Al–20 vol % SiC_p tested at 38.0 MPa, (d) Al–20 vol % SiC_p tested at 44.0 MPa, and (e) Al–30 vol % SiC_p tested at 54.0 MPa.

can be seen in a scanning electron micrograph of the longitudinal section of the crept Al–10 vol % SiC_p sample (Fig. 6), where almost all the cavities are associated with silicon carbide particulates. In addition, necking was observed in the samples tested above the transition stress. Similar fractographical features were observed in Al–20 vol % SiC_p (Fig. 5c and d) and Al–30 vol % SiC_p (Fig. 5e).

From Table I, it can be noted that the strain to fracture, ε_f, increases in all cases with the applied stress, σ. The strain to fracture is 15% for Al–10 vol % SiC_p composite at the applied stress of 30.5 MPa and decreases to $\sim$ 2% at 24.5 MPa. The fracture strain

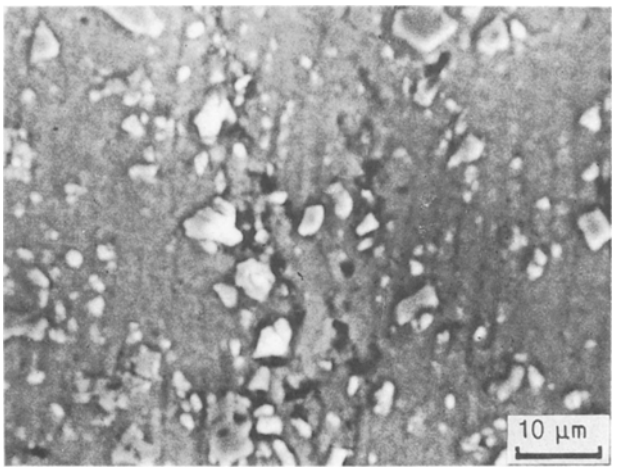

Figure 6 Scanning electron micrograph showing the longitudinal section of a tested Al–10 vol % SiC_p (30.5 MPa) near the fracture end. Note the decohesion around some particles.

decreases with the volume fraction of SiC_p significantly and the least ε_f is 0.37% at the stress of 36 MPa for the Al–20 vol % SiC_p.

4. Discussion

4.1. Creep curves

The shape and the extent of the tertiary part of the creep curve in composites varies considerably with the applied stress and the volume fraction of the SiC reinforcement. At low stresses, the creep curves have a well-defined secondary stage followed by a short tertiary. The low ductility and short tertiary suggest small deformation of the matrix. From the fractographs, these specimens appear to have failed predominantly by intergranular fracture. On the other hand, at higher stresses the tertiary stage follows immediately after the primary stage, and the secondary stage is absent. Higher ductility of specimens at higher stresses, and ductile failure indicate transgranular fracture. This is expected to arise from void nucleation at the Al/SiC interface and subsequent growth and coalescence of these intragranular voids. Hence, the change in the shape of the creep curve is linked primarily with a transition from intergranular fracture to transgranular fracture.

4.2. Transition stress

The transition stress, σ_{tr}, (Table II) varies linearly with the volume fraction, V_f, of SiC

$$\sigma_{tr} = 118.6V_f + 12.6 \quad (1)$$

The data for commercial purity aluminium fit quite well with the reinforced composite data. We note that the reinforcement of aluminium matrix with SiC particulates introduces a threshold stress [17]. The origin of such a threshold stress is thought to be related to the load transfer to the stiffer phase. Therefore, it appears that the increase in transition stress is merely a mechanical shift, because a part of the applied stress, i.e. threshold stress, is not acting on the matrix in the initial stages of the creep test. It should be noted that this value of the threshold stress would decrease with decohesion at the interface during the tertiary stage. However, for the present analysis we are using minimum creep rate data and hence the use of the threshold stress value determined for steady-state creep is reasonable. The normalized effective transition stress is also given in Table II. No general trend is apparent and with the existing scatter we consider the value for normalized effective transition stress to be a constant ($(\sigma - \sigma_o)/G \approx 4.7 \times 10^{-4}$). All the evidence suggests the transition stress to be associated with the transition from intergranular to transgranular fracture. Transgranular fracture occurs by nucleation of cavities at intragranular particles.

A number of models are available for cavity nucleation in dispersion-strengthened materials. Fundamentally, these models either predict a critical strain [19], or a critical strain rate [20] for cavity nucleation. The critical strain approach is based on the concept of work hardening around particles. Brown and Stobbs [19] give the criterion for cavity nucleation as

$$\varepsilon_c > \frac{1}{30}\left(\frac{\sigma_c}{aG}\right)^2 \frac{r}{b} \quad (2)$$

where ε_c is the critical strain produced by the local work hardening at the particle, σ_c is the critical stress, G is the shear modulus, r is the radius of the particle, a is a constant and $\boldsymbol{b}$ is the Burgers vector. From the present results it appears that $\varepsilon_c < 0.003$ because no steady state was observed at higher stresses, i.e. cavities nucleated in the primary stage itself. Taking $\varepsilon_c = 0.3\%$, $G = 21$ GPa at 623 K, $a = 1/7$ [19], $r = 0.85$ μm, $b = 2.86 \times 10^{-4}$ μm, σ_c/G for the nucleation of cavity at the interface is 7.9×10^{-4}. This value is a little higher than the transition stress of 4.7×10^{-4}, but is in line with the argument that the interfacial stresses are higher than the applied stresses because of stress concentration. This value is, however, much lower than the value 1×10^{-2} suggested for Cu–SiO_2 [21].

Koeller and Raj [20] have suggested a strain-rate criterion for cavity nucleation

$$\dot{\varepsilon}_c \geqslant 118\frac{(1-\nu)\,[1-2\nu+(2/\pi)]}{[(5/6)-\nu]^2}\left(\frac{G\Omega}{kT}\right)\left(\frac{V_f \delta D_B}{p^3}\right) \quad (3)$$

where $\dot{\varepsilon}_c$ is the critical strain rate, ν is the Poisson's ratio, Ω is the atomic volume, δ is the boundary width, D_B is the grain-boundary self-diffusion coefficient and p is the particle diameter. This equation has been derived on the basis of interfacial diffusional relaxation of stresses generated at the interface, which indicates that for cavity nucleation to occur, the rate of relaxation has to be slower than $\dot{\varepsilon}_c$ given above. Using values for pure aluminium, $G = 21.0$ GPa at 623 K, $\Omega = 1.66 \times 10^{-29}$ nm^3, $k = 1.38 \times 10^{-23}$ JK^{-1}, $\nu = 0.34$, $\delta D_B = 5 \times 10^{-14} \exp(-84000/RT)$ m^{3}s^{-1} [22], $V_f = 0.1$ and $p = 1.7$ μm, the value of $\dot{\varepsilon}_c$ is 1.3×10^{-6} s^{-1}. In this study, the critical strain rate is $\sim 1 \times 10^{-8}$ s^{-1}, which is almost two orders of magnitude lower than the predicted value. It should be noted that for the above calculations the grain-boundary self-diffusion value for pure aluminium has been taken. This might not be appropriate as the interfacial diffusivity at the Al/SiC interface can be much lower. In an analysis of superplastic data on Al/SiC composites, Mishra and Mukherjee [23] found an activation energy of 313 kJ mol^{-1}. Use of this activation energy in Equation 3 gives a critical strain rate value of 7.6×10^{-26} s^{-1}. It is obvious from this value that diffusional relaxation by interfacial diffusion would not be able to relax the stress concentration. In such a situation lattice diffusion can also contribute to the diffusional relaxation. To evaluate this possibility the term $(\delta D_B/p^3)$ in Equation 3 can be replaced by $(D_v/3p^2)$, where D_v is the lattice self-diffusion coefficient (assuming the same difference as in the diffusional creep by lattice diffusion [24, 25] and grain-boundary diffusion [26], which should be approximately in the same order). Taking $D_v = 1.0 \times 10^{-4} \exp(-142000/RT)$ m^{2}s^{-1} [22], the critical strain rate is 2×10^{-8} s^{-1}. This agrees well with the experimental value.

It is important to note that both the models have different particle-size dependence. Although it is difficult to conclude decisively which model is more appropriate for the transition stress at this stage, because of the lack of data on particle-size dependence, the diffusional relaxation model with lattice diffusion appears to be more appropriate.

4.3. Fracture mechanism

From the SEM fractographs (Fig. 5), the significant difference in the fracture behaviour of the samples tested below and above the transition stress is apparent. Below the transition stress, intergranular creep fracture occurs, whereas transgranular fracture is observed above the transition stress in all cases. This observation is consistent with the fracture mechanism map reported by Ashby *et al.* [27] for commercial purity aluminium (Fig. 7). It can be seen that the range of effective stresses used for composites falls in the region of transition from intergranular to transgranular creep fracture. In spite of this transition, the entire data follow the modified Monkman–Grant relation [28]

$$\dot{\varepsilon}_m \frac{t_f}{\varepsilon_f} = K_o \tag{4}$$

where $\dot{\varepsilon}_m$ is the minimum creep rate, t_f is the time to fracture and K_o is a constant (Fig. 8). The value of K_o for the present data is approximately 0.35. This indicates that both the intergranular fracture and transgranular fracture are controlled by power-law creep.

Cocks and Ashby [29] have given a relation for creep fracture by power-law creep-controlled intergranular void growth as

$$\varepsilon_f = t_f \dot{\varepsilon}_m + 0.2\frac{l}{d} \tag{5}$$

where l is half of the intervoid spacing and d is the grain size. Taking $d = 5$ μm, Equation 5 gives a range of values for l from 60–300 nm for the present data. These values are much less than the interparticle

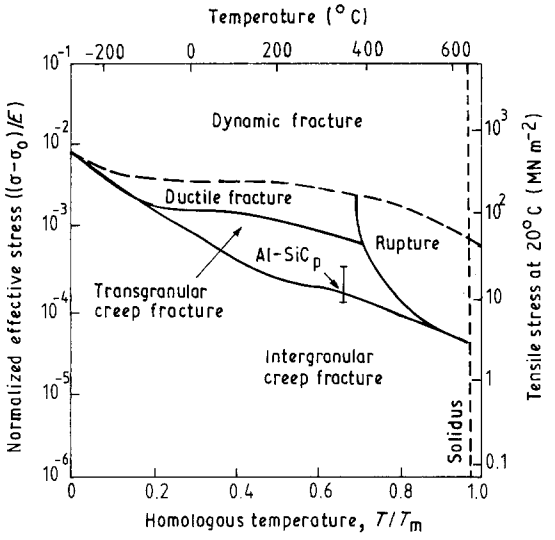

Figure 7 The fracture mechanism map for commercial purity aluminium [27] is shown with the present data. The effective normalized stress is plotted to account for the threshold stress because of reinforcement of the matrix with SiC particulates.

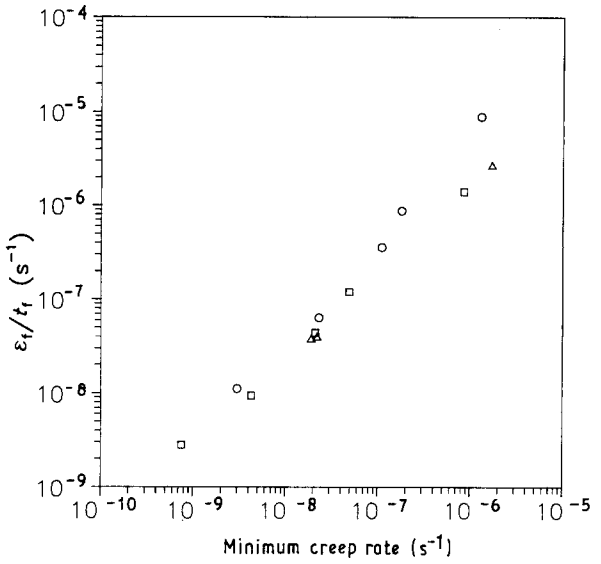

Figure 8 A modified Monkman–Grant plot showing all the fracture data. (○) Al–10 vol % SiC, (□) Al–20 vol % SiC, (△) Al–30 vol % SiC.

spacing of SiC [17]. Hence, the intergranular voids appear to be independent of SiC particulates. This would mean that intergranular fracture in Al–SiC_p composites is similar to that of the unreinforced commercial purity aluminium.

The transgranular fracture in Al–SiC_p composites is linked with local necking between SiC particles. The ductility of Al–SiC_p composites decreases with increasing volume fraction of SiC. Brown and Embury [30] have proposed a model for ductile failure by nucleation of voids at particles and their subsequent growth and coalescence. This model gives

$$\varepsilon_f \equiv \ln (1 + \varepsilon_g + \varepsilon_n) \tag{6}$$

where ε_g is the growth strain and ε_n is the nucleation strain. As mentioned earlier, the nucleation strain appears to be very small and therefore this can be neglected in the above expression. Ashby *et al.* [27] have given an expression for the growth strain as

$$\varepsilon_g \approx \frac{1}{C} \ln \left[a' \left(\frac{1}{V_f^{1/2}} \right)^{-1} \right] \tag{7}$$

where C is a constant with a value of 1.4 [31] and a' is a constant of order unity. Although this can qualitatively explain the volume-fraction dependence of the strain to fracture, it fails on two accounts. Firstly, it overestimates the strain to fracture by several times, and secondly, it does not have any term to explain the observed stress dependence in the present study (see Table I).

5. Conclusions

1. A transition stress exists above which no steady-state stage is observed in Al–SiC composites.
2. The transition stress is related to a transition from intergranular to transgranular creep fracture.
3. The origin of the transition stress is perhaps associated with the diffusional relaxation of stress concentration at the matrix/particle interface by lattice diffusion.

4. The intergranular creep fracture of composites is not linked with SiC particulate distribution and it is power-law creep controlled.

5. The transgranular creep fracture of composites occurs by void nucleation at the SiC particulate interface and their subsequent growth. The early nucleation of voids results in the absence of a steady-state stage.

6. The ductile fracture models overestimate the strain to fracture and do not predict the observed stress dependence of strain to fracture.

Acknowledgement

The authors thank the Director, DMRL, for permission to publish this work.

References

1. A. P. DIVECHA, S. G. FISHMAN and S. D. KARMARKAR, *J. Metals* **33** (1981) 12.
2. A. P. DIVECHA and S. G. FISHMAN, *Sampe Q.* **12** (1981) 40.
3. D. L. McDANELS, *Metall. Trans.* **16A** (1985) 1105.
4. S. V. NAIR, J. K. TIEN and R. C. BATES, *Int. Metall. Rev.* **30** (1985) 275.
5. D.WEBSTER, *Metall. Trans.* **13A** (1982) 1511.
6. T. G. NIEH, *ibid.* **15A** (1984) 139.
7. V. C. NARDONE and J. R. STRIFE, *ibid.* **18A** (1987) 109.
8. T. G. NIEH, K. XIA and T. G.LANGDON, *J. Engng. Mater. Technol.* **110** (1988) 77.
9. T. MORIMOTO, T. YAMAOKA, H. LILHOLT and M. TAYA, *ibid.* **110** (1988) 70.
10. H. LILHOLT and M. TAYA, in "Proceedings of ICCM and ECCM", Vol. 2, edited by F. L. Matthews, N. C. R. Buskell, J. M. Hodkinson and J. Morton, (Elsevier Applied Science, London, UK, 1987) p. 2234.
11. K. XIA, T. G. NIEH, J. WADSWORTH and T. G. LANGDON, in 'Fundamental Relationships between Microstructure and Mechanical Properties of Metal Matrix Composites" (TMS, Warrendale, PA, 1990).
12. E. P. BARTH, J. T. MORTON and J. K. TIEN, *ibid.* (1990).
13. S. PICKARD and B. DERBY, in "Developments in the Science and Technology of Composite Materials", Third European Conference on Composite Materials, France, edited by A. R. Bunsell, P. Lamicq and A. Massiah (Elsevier Science, London UK, 1989) p. 199.
14. S. GOTO and M. McLEAN, *Acta Metall.* **39** (1991) 165.
15. K. T. PARK, E. J. LAVERNIA and F. A. MOHAMED, *Acta Metall. Mater.* **38** (1990) 2149.
16. A. B. PANDEY, R. S. MISHRA and Y. R. MAHAJAN, *Scripta Metall. Mater.* **24** (1990) 1565.
17. A. B. PANDEY, R. S. MISHRA and Y. R. MAHAJAN, *Acta Metall. Mater.* **40** (1992) 2045.
18. R. S. MISHRA and A. B. PANDEY, *Metall. Trans.* **21A** (1990) 2089.
19. L. M. BROWN and W. M. STOBBS, *Phil. Mag.* **34** (1976) 351.
20. R. C. KOELLER and R. RAJ, *Acta Metall.* **26** (1978) 1551.
21. S. H. GOODS and L. M. BROWN, *ibid.* **27** (1979) 1.
22. H. J. FROST and M. F. ASHBY, "Deformation Mechanism Maps" (Pergamon Press, London, 1982).
23. R. S. MISHRA and A. K. MUKHERJEE, *Scripta Metall. Mater.* **25** (1991) 271.
24. F. R. N. NABARRO, in "Report of the Conference on the Strength of Solids" (Physical Society, London, 1948) p. 75.
25. C. HERRING, *J. Appl. Phys.* **21** (1950) 437.
26. R. L. COBLE, *ibid.* **34** (1963) 1679.
27. M. F. ASHBY, C. GANDHI and D. M. R. TAPLIN, *Acta Metall.* **27** (1979) 669.
28. F. DOBES and K. MILICKA, *Metal Sci.* **10** (1976) 382.
29. A. C. F. COCKS and M. F. ASHBY, *Progr. Mater. Sci.* **27** (1982) 189.
30. L. M. BROWN and J. D. EMBURY, in "Proceedings of the 3rd International Conference on the Strength of Metals and Alloys" (Institute of Metals, London, 1973) p. 164.
31. G. LEROY, J. D. EMBURY, G. EDWARD and M. F. ASHBY, *Acta Metall.* **29** (1981) 1509.

Received 2 January
and accepted 2 September 1992